

SiliconPV: 17-20 April 2011, Freiburg, Germany

Formation of locally aluminum-doped *p*-type silicon regions by in-line high-rate evaporation

Christoph Mader^{a,*}, Robert Bock^a, Jens Müller^a, Jan Schmidt^a, Rolf Brendel^{a,b}

^a*Institute for Solar Energy Research Hamelin (ISFH), Am Ohrberg 1, 31860 Emmerthal, Germany*

^b*Institute for Solid State Physics, Leibniz University of Hannover, Appelstrasse 2, 30167 Hannover, Germany*

Abstract

Locally aluminum-doped *p*-type silicon regions are formed by in-line high-rate evaporation of aluminum. We deposit aluminum layers of 28 μm thickness at dynamic deposition rates of 20 $\mu\text{m}\times\text{m}/\text{min}$ on locally laser-ablated Al_2O_3 / SiN_x passivation layers. Due to the high substrate temperature of up to 778°C during deposition an Al-doped p^+ region is formed. Using the camera-based dynamic infrared lifetime mapping technique we determine a contact recombination velocity of 1000 ± 100 cm/s for local Al- p^+ regions on *p*-type silicon wafers of 1.5 Ωcm resistivity. The recombination velocity between the contacts is determined to 4.4 ± 0.5 cm/s after deposition.

© 2011 Published by Elsevier Ltd. Selection and/or peer-review under responsibility of SiliconPV 2011.

Keywords: Crystalline silicon solar cell; in-line evaporation; aluminum doped silicon; alloying; local contacts

1. Introduction

The rear side of a standard industrial-type silicon solar cell is contacted by screen-printing. This process has three steps: (i) An aluminum paste is printed onto the silicon wafer, (ii) the paste is dried at a temperature of $\sim 200^\circ\text{C}$, and (iii) the Al paste is fired in a belt furnace at peak temperatures of $\sim 850^\circ\text{C}$

* Corresponding author. Tel.: +49-5151-999-642; fax: +49-5151-999-400.

E-mail address: mader@isfh.de.

[1]. The firing provides an ohmic contact on the entire rear side and also forms an aluminum-doped p^+ ($\text{Al-}p^+$) region, which reduces the rear surface recombination. As an alternative metalization scheme the in-line high-rate evaporation of aluminum has recently been introduced [2,3]. Similar to the screen-printing, drying and firing process an ohmic contact and an $\text{Al-}p^+$ region is formed by single evaporation of aluminum. In Refs. 2 aluminum layers of up to 28 μm thickness were deposited at dynamic deposition rates of 20 $\mu\text{m}\times\text{m}/\text{min}$. The deposition leads to an increase in wafer temperature due to the enthalpy of deposition. The maximum substrate temperatures during the deposition are well above the eutectic temperature of the Al-Si system and thus are leading to the formation of highly aluminum-doped p -type silicon regions. The $\text{Al-}p^+$ regions are formed on the complete rear side and emitter saturation current densities of (695 ± 65) fA/cm^2 for the fully metalized $\text{Al-}p^+$ regions are determined [2]. This corresponds to an implied solar cell open-circuit voltage of only (635 ± 2) mV thus limiting the energy conversion efficiencies of solar cells. Higher open circuit voltages can be achieved by a passivated and only locally contacted rear side [4,5,6]. In this paper, we present the formation of locally aluminum-doped p -type silicon regions by a single in-line high rate evaporation process without any further temperature treatment.

2. Sample preparation

For the S_{eff} measurements we fabricate asymmetric test structures where both sides are well passivated with a stack of atomic-layer-deposited (ALD) aluminum oxide Al_2O_3 and plasma-enhanced-chemical-vapor-deposited (PECVD) silicon nitride SiN_x . The p^+ region is prepared on one side of the samples by local laser ablation of the dielectric stack and subsequent high-rate Al deposition. For the sample preparation we use 2.5×2.5 cm^2 , single-crystalline, (100)-oriented and 270 μm thick p -type float-zone (FZ) silicon wafers of 1.5 Ωcm resistivity. After KOH etching and RCA cleaning we deposit on both wafer sides a 10 nm thick ALD- Al_2O_3 layer and a 90 nm thick PECVD- SiN_x layer with a refraction index of $n = 2.05$ at a wavelength of $\lambda = 632$ nm [7]. For the single sided contact openings laser pulses of 8 to 9 picoseconds at a wavelength of 532 nm are applied to the samples using a Nd: YVO4 laser. The contacting scheme consists of parallel line contacts with a width of $b = 85$ μm and a period length of $p = 2000$ μm . Finally, we evaporate Al layers of 13, 20, and 28 μm thickness on the locally opened wafer side. The Al deposition process parameters are summarized in Table 1.

Table 1: Dynamic deposition rate r , tray speed v_{tray} and Al layer thickness d of the evaluated processes. The dynamic deposition rate of all processes is fixed at $r = 20$ $\mu\text{m}\times\text{m}/\text{min}$. The variation in Al layer thickness is achieved by different tray speeds.

Process	Dynamic deposition rate r [$\mu\text{m}\times\text{m}/\text{min}$]	Tray speed v_{tray} [m/min]	Al layer thickness d [μm]
1	20	1.5	13
2	20	1	20
3	20	0.7	28

All processes are carried out at dynamic deposition rates of $r = 20$ $\mu\text{m}\times\text{m}/\text{min}$ using an in-line high-rate metalization system (ATON 500 from Applied Materials). Figure 1 shows a sketch of the deposition process. The high deposition rate leads to an increase in the wafer temperature of up to 778°C (simulated). No active heating is applied. We calculate the substrate temperature using two-dimensional finite-element simulations [8,9]. The simulations are based on a simplified model of the heat flows j during evaporation. These heat flows into and out of the wafer are caused by the enthalpy of deposition of aluminum and heat radiation of the wafer.

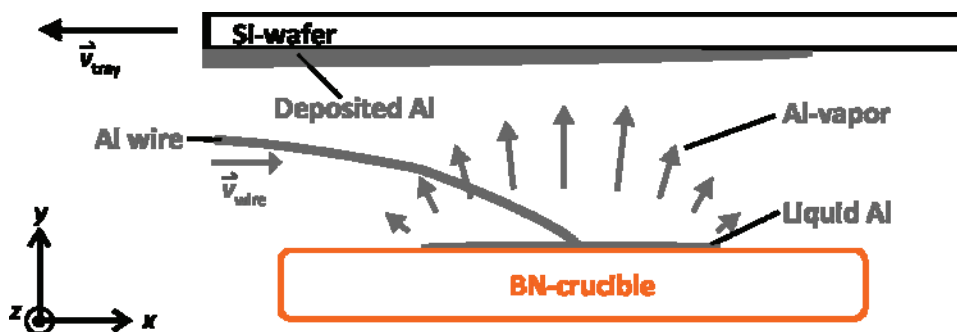


Fig. 1. Schematic sketch of the Al deposition process. An aluminum wire is steered onto heated boron nitride (BN) crucibles, resulting in a continuous generation of aluminum vapor. The evaporated aluminum deposits on the sample that moves on a carrier through the deposition chamber. Many BN crucibles are positioned next to each other in z-dimension to have a homogeneous deposition on a width of 500 mm.

Please note that phase transitions are not considered in the simulation. The simulation has been verified with temperature measurements at deposition processes with a dynamic deposition rate of $r = 5 \mu\text{m}\times\text{m}/\text{min}$ leading to maximum substrate temperatures of 400°C . Simulated and measured peak temperatures agree within 3% [8,9].

3. Experimental results

Figure 2 shows the calculated substrate temperature for three deposition processes with layer thicknesses d of $13 \mu\text{m}$, $20 \mu\text{m}$, and $28 \mu\text{m}$.

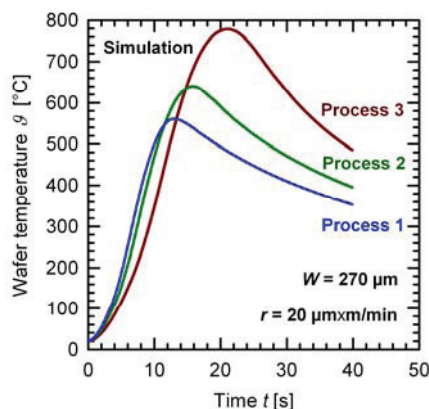


Fig. 2. Substrate temperature θ during deposition of Al layers of various thicknesses d (see Table 1) deduced from numerical simulations. The Si wafer thickness is fixed at $W = 270 \mu\text{m}$. The increase in temperature is caused by the deposition of aluminum.

The deposition of Al layers of $20 \mu\text{m}$ and $28 \mu\text{m}$ on $270 \mu\text{m}$ -thick Si wafers leads to temperatures well above the eutectic temperature of 577°C of the Al-Si system. Thus, an Al- p^+ region forms similar to the screen-printing process. Please note that the temperature during deposition depends on the ratio of wafer thickness W and Al layer thickness d . Using thinner Si wafers at fixed Al layer thickness leads to higher temperatures and thus the formation of an Al- p^+ region is also possible by depositing Al layers $< 10 \mu\text{m}$. The integration of a heater in the deposition system could further decrease the Al layer thickness, which is

required for the formation of an Al- p^+ layer. The high temperature during evaporation improves the passivation quality of the Al₂O₃-SiN_x stack [10,11]. On symmetric reference samples passivated with an Al₂O₃-SiN_x stack we measure surface recombination velocities (SRV) of $S_{\text{Al}_2\text{O}_3} \geq 25$ cm/s before and of $S_{\text{Al}_2\text{O}_3} \leq 5$ cm/s after Al deposition. Effective SRV S_{eff} are obtained from metalized samples using the camera-based dynamic infrared lifetime mapping technique (dyn ILM) [12,13]. We do not observe an injection-dependent lifetime in the range from $\Delta n = 10^{14} - 3 \times 10^{15}$ and extract the effective surface recombination velocities S_{eff} from the measured lifetime at an injection level $\Delta n = 2 \times 10^{15} \text{ cm}^{-3}$ on an area of $2 \times 2 \text{ cm}^2$ using the equation [14]

$$\frac{1}{\tau_{\text{eff}}} = \frac{1}{\tau_{\text{bulk}}} + \frac{S_{\text{Al}_2\text{O}_3}}{W} + \frac{S_{\text{eff}}}{W} \quad (1)$$

where W is the wafer thickness. It is assumed that the excess carrier concentration Δn is uniform throughout the base, which is not strictly valid for large surface recombination velocities. We assume that the bulk lifetime of the substrate is Auger-limited [15]. Figure 3 shows cross-sectional SEM images of the evaporated local Al- p^+ samples of the three deposition processes 1 through 3. The images are obtained from an ultra-high resolution Hitachi S-4800 field emission SEM. The Al-doped p^+ -region appears brighter than the high-resistivity bulk of the silicon wafer due to the potential contrast [16]. Process 1 from Table 1 results in a temperature of $\vartheta_{\text{max}} = 560^\circ\text{C}$, which is below the eutectic temperature of 577°C , thus an Al- p^+ region has not formed [see Figure 3 (a)]. Process 2 results in wafer temperatures of $\vartheta_{\text{max}} = 640^\circ\text{C}$, leading to the formation of an Al- p^+ region. Nevertheless, Figure 3 (b) shows a discontinuous aluminum-doped region. The Process 3 from table 1, where a peak substrate temperature of $\vartheta_{\text{max}} = 778^\circ\text{C}$ has been simulated, results in a completely closed Al- p^+ region within the contact openings as shown in Figure 3 (c). From this SEM image we determine the Al- p^+ depth to be $(5 \pm 3) \mu\text{m}$.

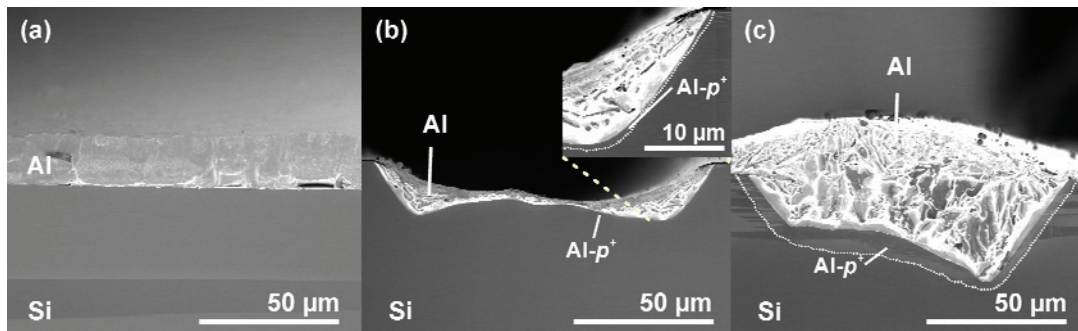


Fig. 3. SEM micrographs of cross sections of samples processed with processes 1–3. The samples feature an Al₂O₃-SiN_x passivation stack with line openings of a width of $85 \mu\text{m}$ before Al deposition. The line width increases during the formation of the Al- p^+ layer to $120 \mu\text{m}$. (a) SEM micrograph of a sample processed with process 1. The process temperature below 577°C is not leading to a local Al- p^+ region. (b) Process 2 results in a higher maximum wafer temperatures of $\vartheta_{\text{max}} = 640^\circ\text{C}$, leading to the formation of a discontinuous Al- p^+ region represented by the dotted line. The emitter thickness is $(150 \pm 150) \text{ nm}$. The Al- p^+ region is clearly visible as brighter contrast. (c) Process 3 ($\vartheta_{\text{max}} = 778^\circ\text{C}$) results in a completely closed Al- p^+ region as represented by the dotted line. The emitter thickness is $(5 \pm 3) \mu\text{m}$.

At temperatures above the eutectic temperature silicon dissolves into the aluminum layer. The passivation layer acts hereby as a diffusion barrier and the alloying process can only take place in the area of the local openings. This results in the surface morphology shown in Fig. 6 (b) and (c). Please note, that the width of the line contacts after the formation of the Al- p^+ region increases to $b = 120 \mu\text{m}$. A detailed analysis of the contact formation of local Al alloyed Si contacts is given in Ref. [17]. Figure 4 shows the measured rear SRV S_{eff} depending on Al layer thickness. Process 1 (see Table 1) with an Al layer thickness of $13 \mu\text{m}$ is not leading to the formation of an Al- p^+ region. The corresponding recombination velocity is $S_{\text{eff}} = (114 \pm 15) \text{ cm/s}$. Processes 2 and 3 (see Table 1) lead to the formation of an Al- p^+ region and are thus reducing the effective SRV. Process 2 results in a SRV of $(99 \pm 10) \text{ cm/s}$ and process 3 in a value of $(50 \pm 5) \text{ cm/s}$. Latter value is in the same range as published SRVs of screen-printed local Al- p^+ regions [6].

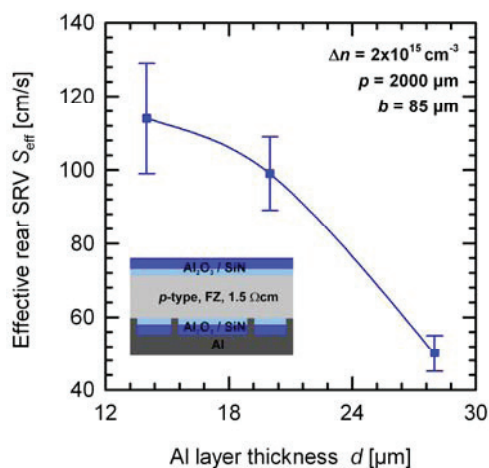


Fig. 4. Measured effective surface recombination velocity as function of the Al layer thickness d of a $1.5 \Omega\text{cm}$ FZ p -Si wafer. One side of the wafer is passivated with a stack of Al_2O_3 and SiN_x . The other side is passivated with the same stack and features local laser openings of a width of $85 \mu\text{m}$ and a period length of $2000 \mu\text{m}$. The local Al- p^+ region forms at the interface of Al to Si in the area of the laser openings.

We extract the contact recombination velocity S_{cont} from the measured S_{eff} values using equation [18]

$$S_{\text{eff}} = \left(\frac{R_s - \rho W}{\rho D} + \frac{1}{f S_{\text{cont}}} \right)^{-1} + \frac{S_{\text{pass}}}{1 - f} \quad (2)$$

where R_s is the series resistance of the majority carriers in the bulk, ρ is the base resistivity, W the sample thickness, D the diffusion coefficient and f the metallization fraction. S_{pass} is the surface recombination velocity between and S_{cont} the surface recombination velocity under the contacts. Using equation 2 we determine $S_{\text{cont}} = (7 \pm 2) \times 10^3 \text{ cm/s}$ for process 1. Processes 2 and 3 are reducing the contact recombination velocity to values of $(3 \pm 0.5) \times 10^3 \text{ cm/s}$ and $(1 \pm 0.1) \times 10^3 \text{ cm/s}$, respectively.

4. Conclusion

In conclusion, we have presented results on in-line high-rate evaporation of aluminum on silicon substrates. Using numerical simulations, we have shown that the deposition process leads to temperatures of $T_{\max} = 778^{\circ}\text{C}$. These conditions lead to the formation of an Al- p^+ region without any further temperature treatment. We determine a contact recombination velocity of 1000 ± 100 cm/s for local Al- p^+ regions on silicon wafers of $1.5 \Omega\text{cm}$ resistivity resulting in an effective surface recombination velocity of only (50 ± 5) cm/s for a typical rear contacting scheme with a line width of $b = 85 \mu\text{m}$ and a period length of $p = 2000 \mu\text{m}$.

Acknowledgements

This work is supported by the State of Lower Saxony.

References

- [1] Ralph E. Recent advancement in low cost solar cell processing. Proceedings of the 11th IEEE Photovoltaic Specialists Conference 1975; Scottsdale: 315 - 316.
- [2] Mader C, Bock R, Schmidt J, Brendel R. Formation of highly aluminum-doped p -type silicon regions by in-line high-rate evaporation. *Sol. Energy Mater. Sol. Cells* 2011, doi:10.1016/j.solmat.2011.01.039.
- [3] Mader C, Bock R, ISFH, Patent pending.
- [4] Agostinelli G, Choulat P, Dekkers H, De Wolf S, Beaucarne G. Screen printed larg area crystalline silicon solar cells on thin substrates Proceedings of the 20th European Photovoltaic Solar Energy Conference (WIP, Barcelona, 2005). pp. 647-650.
- [5] Ramanathan S, Das A, Cooper I, Rohatgi A, Payne A, Koehler I. 20% efficient screen printed LBSF cell fabricated using UV laser for rear dielectric removal. Proceedings of the 35th IEEE Photovoltaic Specialists Conference (IEEE, Hawaii, 2010). pp. 678-682.
- [6] Gatz S, Hannebauer H, Hesse R, Werner F, Schmidt A, Dullweber T, Schmidt J, Bothe K, Brendel R. 19.4%-efficient large-area fully screen-printed silicon solar cells. *Phys. Status Solidi RRL* (2011) **5**, No. 4, 147–149.
- [7] Lauinger T, Schmidt J, Aberle AG, Hezel R. Record low surface recombination velocities on $1 \Omega\text{cm}$ p -silicon using remote plasma silicon nitride passivation. *Appl. Phys. Lett.* 1996; **68**: 1233.
- [8] Mader C, Eitner U, Brendel R. Experimentelle Untersuchungen und Simulationsrechnungen zur Temperaturentwicklung bei Hochraten- Aufdampfprozessen. *Workshop "Hochratenverdampfen für die Photovoltaik"* 2009; Hameln.
- [9] Mader C, Eitner U, Kessler M, Brendel R. Temperature of silicon wafers during in-line high-rate evaporation of aluminum. *Sol. Energy Mater. Sol. Cells*, submitted.
- [10] Hoex B, Heil S, Langereis E, van de Sanden M, Kessels W. Ultralow surface recombination of c-Si substrates passivated by plasma-assisted atomic layer deposited Al_2O_3 . *J. Appl. Phys.* 2006; **89**: 042112.
- [11] Schmidt J, Merkle A, Brendel R, Hoex B, van de Sanden M, Kessels W. Surface passivation of high-efficiency silicon solar cells by atomic-layer-deposited Al_2O_3 . *Prog. Photovolt: Res. Appl.* 2008; **16**:461–466.
- [12] Ramspeck K, Reissenweber S, Schmidt J, Bothe K, Brendel R. Dynamic carrier lifetime imaging of silicon wafers using an infrared-camera-based approach. *Appl. Phys. Lett.* 2008; **93**: 102104.
- [13] Müller J, Bothe K, Gatz S, Haase F, Mader C, Brendel C. Recombination at laser-processed local base contacts by dynamic infrared lifetime mapping. *J. Appl. Phys.* 2010;**108**; 124513.
- [14] Kane DE, Swanson RM. Measurement of the emitter saturation current by a contactless photoconductivity decay method. Proceedings of the 18th IEEE Photovoltaic Specialists Conference; Las Vegas: 578.
- [15] Kerr M, Cuevas A. General parameterization of Auger recombination in crystall. silicon. *J. Appl. Phys.* 2002; **91** : 2473.
- [16] Sealy CP, Castell MR, Wilshaw PR. Mechanism for secondary electron dopant contrast in the SEM. *Journal of Electron Microscopy* 2000; **49**: 311-321.
- [17] Müller J, Bothe K, Gatz S, Plagwitz H, Schubert G, Brendel R. Recombination at local aluminum alloyed silicon solar cell base contacts by dynamic infrared lifetime mapping. *Energy Procedia*, 1st SiliconPV 2011, Freiburg.
- [18] Fischer B. Loss analysis of crystalline silicon solar cells using photoconductance and quantum efficiency measurements. PhD thesis, Cuvillier, Göttingen 2003.